Acta Astronautica 202 (2023) 863–875

Contents lists available at ScienceDirect

Acta Astronautica

journal homepage: www.elsevier.com/locate/actaastro

Global trajectory optimization, pathfinding, and scheduling for a multi-flyby, multi-spacecraft mission

Ryan P. Russell[1], Sean McArdle [*,2], David Ottesen[2], Enrico M. Zucchelli[2], William E. Brandenburg[2]

The University of Texas at Austin Department of Aerospace Engineering and Engineering Mechanics, 2617 Wichita Street, Austin, 78712-1221, TX, USA

ARTICLE INFO

Keywords:
Global Trajectory Optimization
Lambert problem
Indirect optimization
Genetic algorithms
Dyson ring

ABSTRACT

The UT Austin team presents their methodology and result for GTOC11, constructing a hypothetical Dyson ring using asteroids encountered by 10 motherships departing from Earth. A pathfinding algorithm for the mothership is designed using a fast lookup table and a robust Lambert solver. Sequencing of unique mothership itineraries is performed by approximating the mass delivered to the ring via a linear data-based estimator trained on simulated asteroid-to-ring trajectories. A detailed derivation for the necessary boundary conditions of the constant-thrust-acceleration indirect optimization problem is presented, with key insights about the magnitudes of the co-states. An indirect boundary value solver finds feasible asteroid-to-ring trajectories for each of the 12 phasing locations in a high-performance parallel computing environment. A genetic algorithm informs the sequencing for the ring station arrival order that gives the highest performance index value. UT Austin's final submitted solution placed 4th in the competition, with a performance index value of 5885.5, 235 asteroids collected, and a minimum build-station mass of 1.1328×10^{15} kg.

1. Introduction

The Global Trajectory Optimization Competition (GTOC) is a proving ground for the development of space trajectory optimization tools. The University of Texas at Austin (UT Austin) participated in the 11th edition of GTOC in Fall 2021 [1]. The UT Austin team's solution methodology includes a variety of new techniques that may be generally useful in trajectory optimization, mission design, and space situational awareness.

GTOC is an international competition for practitioners in global trajectory design [2], originally organized in 2005 by Dario Izzo at the European Space Agency's Advanced Concepts Team [3]. For each GTOC event, teams are self-assembled from a diverse set of institutions including industry, universities, space agencies, national laboratories, and individuals. The teams compete to produce optimized solutions for a complex global trajectory design problem. Details of the solution methodology for each GTOC round are shared in workshops and disseminated in special issues of academic journals to foster innovation and collaboration in the mission design community [1,3,4]. A new GTOC is conducted every one-to-two years by the winning team from the previous competition. The host of GTOC11 is the winner of GTOC10: the team from The National University of Defence Technology and The Xi'an Satellite Control Center [4].

According to the GTOC11 problem statement, teams must design a mission to construct a Dyson ring. A Dyson ring is a hypothetical power generation system that captures solar energy using a heliocentric ring of satellites. In GTOC11, the Dyson ring is constructed by accumulating a selection from over 83000 available asteroids. Up to 10 motherships depart from the Earth to rendezvous with selected asteroids. Selected asteroids are sent to one of 12 Dyson ring build-stations using a constant-thrust-acceleration asteroid transfer device (ATD) dropped off by a mothership.

The overall performance index for GTOC11 is specified as

$$J = B\frac{10^{-10}M_{\min}}{a_{\text{Dyson}}^2\sum_{k=1}^{10}\left(1+\Delta v_k^{\text{Total}}/50\right)^2} \tag{1}$$

where B is a score modifier based on the time of submission, $M_{\min}$ is the total accumulated mass at the build-station with the least mass, a_{Dyson} is the semi-major axis of the build-station orbit, and $\Delta v_k^{\text{Total}}$ is the total accumulated Δv for mothership k. The competition hosts provide a comprehensive description of the problem in Ref. [1].

* Corresponding author.
E-mail addresses: ryan.russell@utexas.edu (R.P. Russell), seanmcardle14@utexas.edu (S. McArdle), davidottesen@utexas.edu (D. Ottesen), enricomarco@utexas.edu (E.M. Zucchelli), william.brandenburg@austin.utexas.edu (W.E. Brandenburg).
[1] Professor.
[2] Graduate student.

https://doi.org/10.1016/j.actaastro.2022.07.007
Received 29 April 2022; Received in revised form 29 June 2022; Accepted 5 July 2022
Available online 8 July 2022
0094-5765/Published by Elsevier Ltd on behalf of IAA.

The UT Austin team employs various new techniques that may be useful contributions to the literature. The first contribution is a novel spatial and temporal grid utilizing "bounding boxes" for efficient nearest-neighbor searches. The second contribution is a globally optimal strategy for selection of impulsive maneuvers at the leg boundaries of multiple-flyby tours constrained by a maximum excess velocity. The third contribution is the application of a linear data-based estimator to select the most promising mothership trajectory sequences. The fourth contribution is the derivation of necessary conditions for a variety of indirect trajectory optimization problems and the insight that motion is invariant to the co-state magnitude for constant-thrust acceleration. The final contribution is a scheduling strategy that distributes asteroid mass between the build-stations using a genetic algorithm to select the order of build-station construction. Details on each of these contributions, respectively, are provided in the following paragraphs.

A new "bounding box" technique is introduced to facilitate mothership-to-asteroid trajectory selection. Rather than searching for transfers between each mothership and all 83000+ asteroids on each asteroid-to-asteroid leg of the mothership trajectory, the bounding box technique locates a subset of nearest-neighbor asteroids on a precomputed spatial and temporal grid. Only the nearest-neighbors are considered for transfers. Nearest neighbors are determined by using precomputed ephemerides of all asteroids. A new, globally-robust Lambert solver is used to determine reachability for the mothership trajectory [5,6]. This new bounding box look-up strategy may be useful for future multiple asteroid/comet problems, space debris avoidance and/or mitigation, or coordinated constellation design.

Bounding maneuvers between legs of the multiple-impulse mothership trajectory are calculated by simultaneously considering the impulsive maneuver Δv required to perform the near-rendezvous (constrained by a maximum excess speed) with the current asteroid and the impulsive maneuver Δv required to transfer to the next asteroid. This technique may be useful for other applications, such as interplanetary trajectory design, moon-tour design, satellite constellation servicing, or space debris management.

A data-based linear estimator, trained using data from initial runs, is used to choose 10 motherships from a large set of feasible candidate mothership trajectory sequences. A fast estimation scheme allows many more mothership trajectory sets to be considered than would be possible to test by explicitly generating full solutions. This data-based linear estimation technique is a useful model reduction scheme applied to this expensive multiple asteroid trajectory design problem.

Necessary conditions are derived for a variety of different indirect optimization problems relevant to GTOC11 and other spaceflight applications. A set of necessary conditions is derived for minimum-time-of-flight constant-thrust-acceleration transfers from one Keplerian orbit to another, leaving the initial and final times free. Another set of necessary conditions is derived for transfers with either the initial or the final time held fixed. The motion is shown to be invariant to the magnitude of the co-state as a consequence of the constant-thrust acceleration, and the minimum-time-of-flight necessary conditions require that the initial and final velocity co-state magnitudes are equal. The derivations and insights are relevant to the broad literature concerning indirect spacecraft trajectory optimization.

A new scheduling technique is used to assign all asteroids that have been encountered by the mothership to build-stations, with the goal of distributing mass as evenly as possible. A genetic algorithm is implemented as an outer loop to the asteroid-to-build-station scheduling scheme in order to select a build-station order that globally optimizes the overall GTOC11 performance index from Eq. (1).

The remainder of the paper is organized as follows. A brief preliminary analysis of the GTOC11 problem is presented with a focus on insights that guided the UT Austin team's approach. The mothership-to-asteroid trajectory search is explained, including descriptions of the bounding box spatial and temporal grid strategy, the search for low-Δv mothership-to-asteroid trajectory itineraries, and the use of a linear estimator to select from a large set of candidate mothership-to-asteroid trajectory itineraries. The asteroid-to-ring trajectory solver is then presented, including a derivation of the necessary conditions using an indirect method, an overview of the resulting two-point boundary value problem (TPBVP) solver, and an explanation of the scheduling scheme and genetic algorithm used to match selected asteroids with the available build-station orbits. The final submitted solution from the UT Austin team is presented in detail. Finally, the concluding remarks include a discussion on areas where the solution methodology could be improved.

2. Methods

The solution to the GTOC11 problem is generated by selecting mothership trajectories, solving for constant-thrust-acceleration transfers between each encountered asteroid to the build-stations, and determining the build-station destination for each encountered asteroid. The overall solution generation process is repeated for a grid search over the build-station semi-major axis a_{Dyson}.

2.1. Preliminary analyses

Many irreversible decisions are made at the beginning of any design process. To mitigate early mistakes and focus efforts on high-impact areas, several preliminary analyses were performed to qualitatively map and understand the design space prior to designing and committing to a complete solution method. Key questions sought to be answered at this preliminary stage include: What are the driving input parameters? Which input parameters have the largest impact on the desired output? Can any of the input parameters be decoupled and optimized separately? Are there large portions of the design space that can be efficiently eliminated without significant performance penalty? How many asteroids are expected to be captured? What is the expected cost of each asteroid? Is it better to focus on large asteroids, more asteroids, or less Δv cost per asteroid?

A prudent first step for this global optimization problem is to determine the sensitivities to the performance index with respect to design inputs. Accordingly, several sensitivity analyses are conducted to assess the relative importance of main design parameters [7]. The design space is large, including masses, Δv costs, Dyson-ring radius, and number of asteroids, N_a. To simplify the design space, the functional form of the performance index is considered in the case that (1) all mothership itineraries have the same number of asteroids and same $M_{\min}$, and (2) each asteroid Δv_a cost is identical:

$$\bar{J} = B\frac{10^{-11}M_{\min}}{a_{\text{Dyson}}^2\left(1+\frac{\Delta v_a N_a}{50}\right)^2} \tag{2}$$

This simplified performance index in Eq. (2) is illustrated for fixed $B = 1$ and fixed $M_{\min}$ in the left side of Fig. 1. The dashed red box is the region where most of the best mothership solutions exist, although the location of this box was unknown at the preliminary design stage. Therefore, intuition from prior experience and very preliminary trajectory designs were used to bound feasible regions for $\{\Delta v_a, N_a\}$. The steepest ascent arrows are perpendicular to the contours revealing the directions where the performance index change is most efficient. In the red dashed box, the performance index benefits from both a reduction in Δv_a and an increase in N_a, although the relative importance of N_a diminishes compared to Δv_a as N_a increases. In fact, other regions of the plot (outside of the red dashed box) demonstrate the counter-intuitive result that the performance index actually decreases with more asteroids. Eq. (2) has an analytical maximum when $N_a = 50/\Delta v_a$ (see red curve on right of Fig. 1). Therefore, if each asteroid costs $\Delta v_a = 1$ km/s to capture, then one can capture up to 50 asteroids before the performance index begins to decrease. Similarly, if each asteroid costs $\Delta v_a = 2.5$ km/s to capture, then the performance index begins to

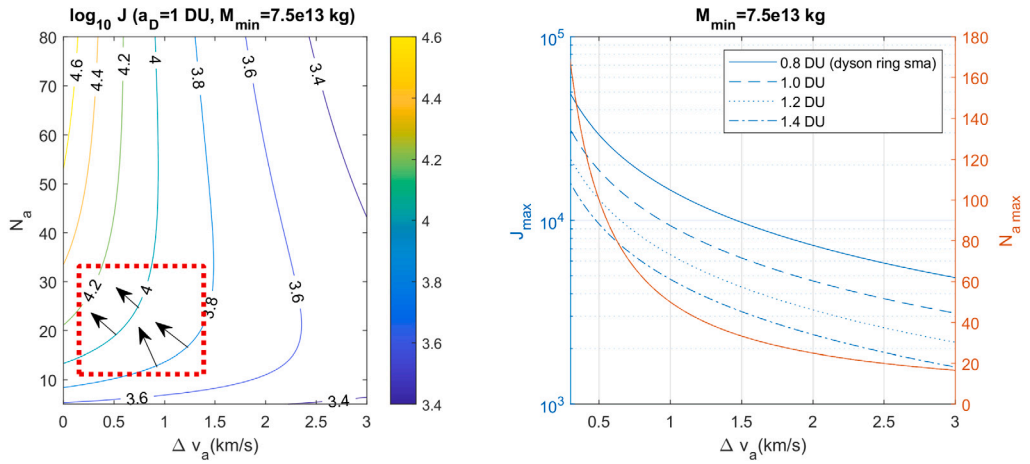

Fig. 1. Analysis of simplified performance index from Eq. (2) to quantify the sensitivity to number of asteroids per mothership and Δv cost per asteroid. (For interpretation of the references to color in this figure legend, the reader is referred to the web version of this article.)

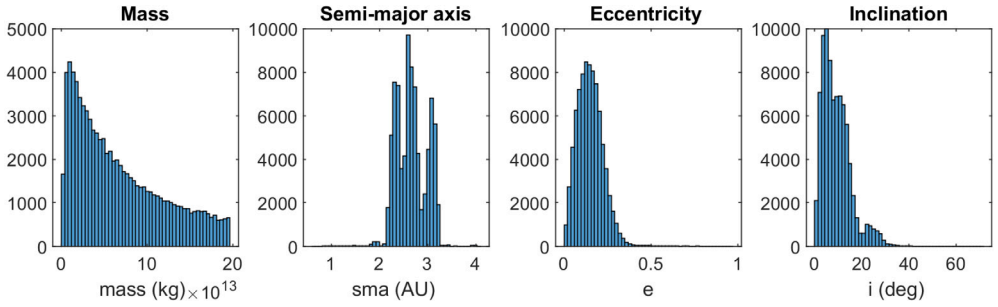

Fig. 2. Histograms for important parameters of the 83453 asteroids.

decrease when $N_a > 20$. Substituting this maximum value of N_a into Eq. (2) yields the maximum possible J as function of Δv (see blue curves on right of Fig. 1). Plots like those in Fig. 1 provide estimates for theoretical ceilings on the performance index. In concert with validated solutions from competing teams on the GTOC scoreboard, such estimates are exploited to efficiently prune the design space.

Fig. 2 shows the distributions of asteroids via histograms for mass, semi-major axis, eccentricity, and inclination. Each histogram uses 50 equally-spaced bins. The asteroid masses vary by an order of magnitude, leaving a clear incentive to target higher masses. However, the large mass asteroids are confirmed to have a near uniform distribution in the position space, and the bulk of the asteroids are small. Therefore, the question of whether to target many small asteroids or few large asteroids remains open. The inclination histogram shows that most asteroids are near the fundamental plane. The eccentricity indicates that asteroids have low to medium eccentricities. These histograms, combined with a simple average (not shown for brevity) of all asteroid orbital planes and eccentricity vectors confirm that a circular and equatorial Dyson ring is a justified and reasonable design choice. Several experiments selecting non-zero values of i_{Dyson} (build-station inclination), Ω_{Dyson} (build-station right ascension of the ascending node), and $\phi_{\text{Dyson},1}$ (initial build-station argument of latitude) did not yield improvements to the overall performance index, so the design space over these three parameters was not further explored.

The semi-major axis histogram is the most informative in Fig. 2, revealing a primarily trimodal distribution. Because the semi-major axis of the Dyson ring appears quadratically in Eq. (1), there is a huge incentive to choose a small value. However, the asteroid transfer from its original orbit is more expensive for larger excursions in semi-major axis. Therefore, the trimodal distribution provides at least two natural choices to filter for maximum asteroid semi-major axis at the dips around 2.5 AU and 2.8 AU. For the final solution, the team did use a simple filter restricting semi-major axis to be less than 2.8 AU. While this filter does significantly reduce the search space, there is also a risk that some high performing asteroids will be missed.

2.2. Mothership trajectory search

The team quickly assessed that the maximum 10 motherships should be utilized. Considering that the motherships are only loosely coupled by the requirement to avoid repeat asteroids, a parallel strategy is adopted to independently populate a list of feasible mothership itineraries, then solve the problem of selecting the subset of 10 separately. This section describes the effort to populate this list of feasible complete mothership trajectories. Based on prior experience with GTOC and similar mission design problems, the preliminary search for the mothership trajectories is anchored on fast, Lambert problems that yield two-impulse transfers with ballistic arcs between asteroids (including Earth).

2.2.1. Time and space discretization

As a first step, fast ephemerides [8] for the Earth and asteroids are precomputed by discretizing the full 20 years of the problem time span into 2000 increments (approximately 3.65 days each). The positions and velocities for the Earth and each of the asteroids are precomputed and stored in a binary file for quick reading and runtime retrieval. Next, the physical configuration space of the problem is discretized into uniform bins in spherical coordinates. This choice of coordinates is natural because the majority of the asteroids are near the equator and an exclusion zone exists close to Sun. The final configuration uses 24, 144, and 36 bins in the radial, longitude, and latitude directions, respectively, totaling 124416 bins spanning 0.35 to 5.0 AU in the radial direction, the full 2π radians in longitude, and $-\pi/4$ to $\pi/4$ radians in latitude.

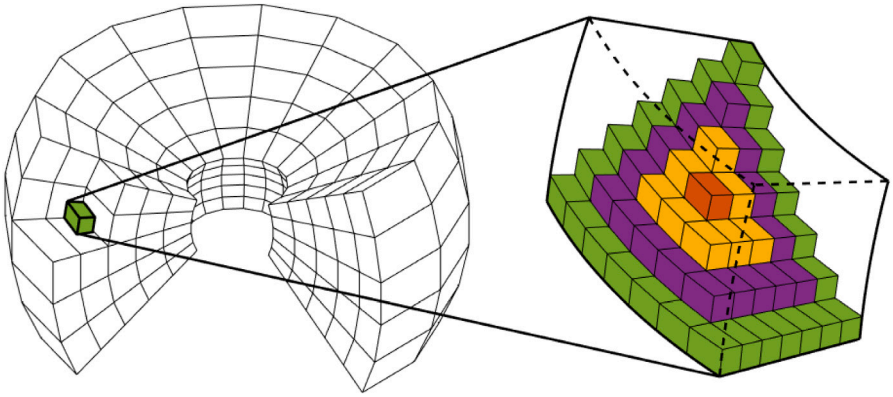

Fig. 3. Solar system discretization via bounding boxes. Left: coarse spherical grid of potential asteroid locations, Right: zoomed-in grid of individual cells, highlighting levels of nearest neighboring cells. (For interpretation of the references to color in this figure legend, the reader is referred to the web version of this article.)

The left side of Fig. 3 illustrates a representative slice of the bins in Cartesian coordinates. To quickly assess which bins are in close proximity to a given bin, a bounding box scheme is devised. The right side of Fig. 3 shows three levels of the bounding boxes encompassing an example center orange bin. The qth-level bounding box contains $(2q+1)^3$ bins, including the central bin. The yellow, purple, and green bins, respectively, represent the $q = 1$, 2, and 3 neighbor levels containing 27, 125, and 343 bins. For fast lookups of items in spatial proximity, an integer list of the indices for each of the q-level neighboring bins is precomputed and archived for each of the 124416 bins. Finally, at each of the precomputed 2000 time increments, each of the asteroid locations is presorted into one of the 124416 bins. Therefore, at the expense of a few GB of memory, a system is in place to rapidly determine what asteroids are close (i.e. less than q bins away) to an arbitrary (mothership) location at any of the time increments. Note that, because the bins are uniform in spherical coordinates, the bin lookup for a given mothership location requires just one float-to-integer conversion for each of the 3 dimensions and a single Cartesian-to-spherical transformation. Otherwise, retrieval of the list of the qth-level neighboring asteroids uses only precomputed lists and pointers.

2.2.2. First asteroid selection

The transfer from Earth to the first asteroid is treated differently than the search for successive asteroid transfers in a candidate mothership itinerary. The first asteroid is handled via an all-on-all strategy where every asteroid is considered with each of the first N time step launch options at Earth. Only time steps during the first 2 years are considered acceptable for launch, considering that earlier launches provide longer flight times with improved opportunities of each mothership. The times-of-flight considered for this initial leg are significantly longer than subsequent legs to enable the mothership to quickly reach the outer asteroid regions, fully exploiting the available 6 km/s excess speed at launch. Recall that all times for the whole problem, including this initial leg, are discretized by the same 2000 points. Each of the all-on-all options is computed via the Lambert solver [6] and the solutions are ranked for each time step according to the total cost to reach the asteroid, accounting for the specified maximum launch and asteroid excess velocities. Therefore, a ranked list of candidate first asteroid targets is precomputed for each candidate launch time step. These lists are archived for fast retrieval to facilitate initiation of the mothership trajectories. Two integer decision variables are required to fully determine an initiation: the ith time step and the jth ranked option, where the latter specifies the first asteroid ID and the arrival time step.

2.2.3. Second-through-N asteroid selection

Upon arrival at the first asteroid, the process is initiated to select the next target. The first step is to filter candidate targets. The bounding box scheme from Fig. 3 is utilized to identify asteroids in spatial proximity to the projected mothership trajectory. Prior to the arrival at the initial body for this ith leg, a pre-arrival collinear maneuver is assumed to take place to satisfy the maximum excess velocity constraint ($v_\infty \leq$ 2 km/s). This post-maneuver arrival condition is the assumed initial condition for a ballistic forecasted mothership trajectory, predicted for n time steps. At each time step, the qth level bounding boxes to the current mothership location are identified, and the encompassing asteroids are noted. The union of each time step's list of asteroids is maintained as a reachable set of potential next target asteroids. For illustration, Fig. 3 shows the bin containing the mothership (orange) at a given time step along with encompassing yellow, purple, then green bins forming the $q = 1$, 2, and 3 bounding boxes, respectively. The q-level is a user input to control how many candidate asteroids pass the filter. In the final runs with the chosen level of spatial discretization, $q = 1$, or occasionally $q = 2$, were found to sufficiently isolate the good asteroid candidates.

Fig. 4 shows a notional diagram of a mothership trajectory and one asteroid, where the bounding boxes at each time step are highlighted if the asteroid resides in the mothership bounding box. Across a single leg of a forecast mothership trajectory, on the order of 10 to 100 asteroids may intersect the bounding box at least once. Fig. 4 is notional to illustrate a single asteroid and its proximity to the mothership, and Fig. 5 shows mothership forecasted legs with true-to-scale depictions of the asteroid, mothership, and bounding box locations.

Because the mothership must nearly rendezvous with potential asteroids, an additional velocity filter is imposed to eliminate unreachable asteroid targets. A phase-free filter using just a normalized difference between the mothership and each asteroid's angular momentum and eccentricity vectors is found to be efficient and fast. These vectors are precomputed for each asteroid, and the mothership vectors can be computed just once per leg. The angular momentum ($\mathbf{h}$) and eccentricity ($\mathbf{e}$) differences are mapped to a proxy for Δv using Eq. (3),

$$\Delta v_* = \alpha \left(\beta_h \left\| \mathbf{h}_a - \mathbf{h}_m \right\| + \beta_e \left\| \mathbf{e}_a - \mathbf{e}_m \right\| \right) \tag{3}$$

where Δv_* is an estimate for the upper bound of the minimized phase-free two-impulse cost to transfer from a mothership (subscript m) to an asteroid (subscript a). The parameters α, β_h, and β_e are chosen using the results of phase-free orbit transfers between thousands of sample asteroids. When canonical units are used, $\alpha = 0.18375$ and the weighting parameters of $\beta_h = 1$ AU^{-1} and $\beta_e = 1$ AU/TU are found to be suitable. These parameters are tuned such that the full fidelity Δv will be greater than the Δv_* lower bound estimate for all or nearly all of the orbit

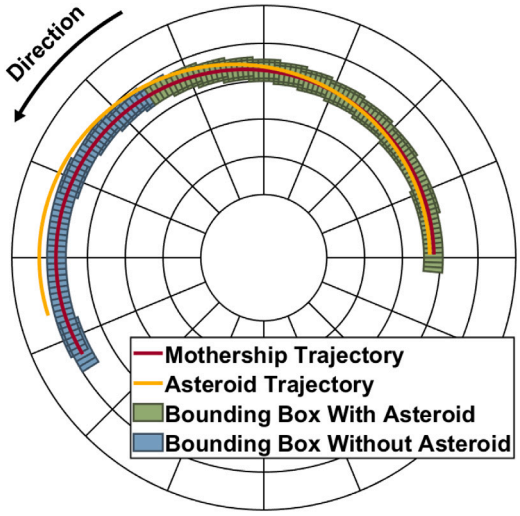

Fig. 4. One leg of a forecasted mothership trajectory and one representative close proximity asteroid.

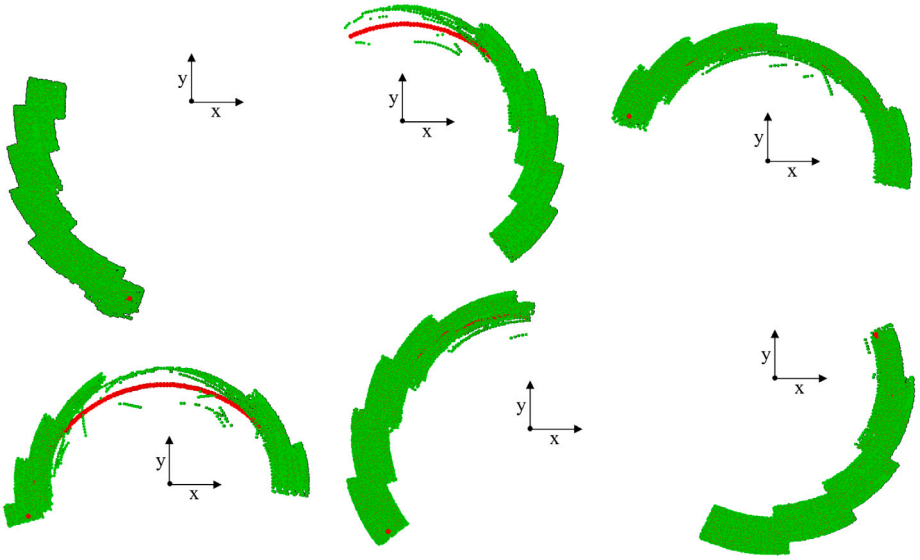

Fig. 5. Mothership segments illustrating the bounding boxes. Large red dots: mothership; Large green dots: candidate asteroids; Light brown dots: asteroids that pass the phase-free filter. (For interpretation of the references to color in this figure legend, the reader is referred to the web version of this article.)

transfers. By enforcing Δv_* to be less than ~2 km/s, this geometric filter typically reduces the number of candidate asteroids by more than half.

Once the final list of potential next-asteroid targets is established, each candidate is considered over a one-dimensional optimization problem, varying flight time and minimizing the total Δv of the potential leg. The range of flight times is limited to a user-specified maximum, on the order of half a year. The optimization is performed via a 1D grid search over the already discretized time-steps, where each feasible flight time requires a single call to the zero-revolution Lambert solver.

The initial Δv on the leg is computed using the strategy depicted in Fig. 6, providing the global minimum Δv solution for a flyby of a non-gravitating body with a maximum excess speed constraint ($v_\infty \leq 2$ km/s). The presumed terminal Δv on the potential leg is computed in the same way as described in the Earth-to-first-asteroid case. The total Δv for each flight time of the potential leg is computed as the sum of the initial and terminal parts. This total Δv is minimized over flight time. Interestingly, the minimized solution rarely coincides with a flight time corresponding to a physical close approach. Instead, these zero-revolution solutions (usually with transfer angles less than 180 degrees) almost always reduce total Δv with longer flight times. Therefore, the user-specified maximum allowable leg flight time is a critical parameter, as most of the minimum total Δv solutions exist on this boundary. Nonetheless, the Δv cost to reach each candidate asteroid target is computed with a 1D grid search requiring on the order of 10 to 100 Lambert calls. The minimized Δv and associated flight time for each candidate asteroid target is recorded.

A cost-to-go model then is adopted to assign a rank to each of the candidate asteroids, assuming that all 10 motherships are identical to the current one, and that all the remaining legs are identical to the current candidate leg. This cost-to-go performance index from Eq. (1) is computed for each candidate target, using the accurate Δv and asteroid masses of completed prior legs but assuming all future legs have the same Δv and mass as the current candidate leg. This approach provides a direct method to weigh the relative importance of the mass, Δv, and flight time costs for reaching each of the candidate targets. Finally, each candidate is assigned a unique rank according to its sorted cost-to-go. The selection of the next target proceeds with a single integer decision variable to choose either the rank 1 option, rank 2 option, …, or rank N option. Once a candidate target is selected for the next leg, the process is repeated for successive legs until the maximum end date is reached.

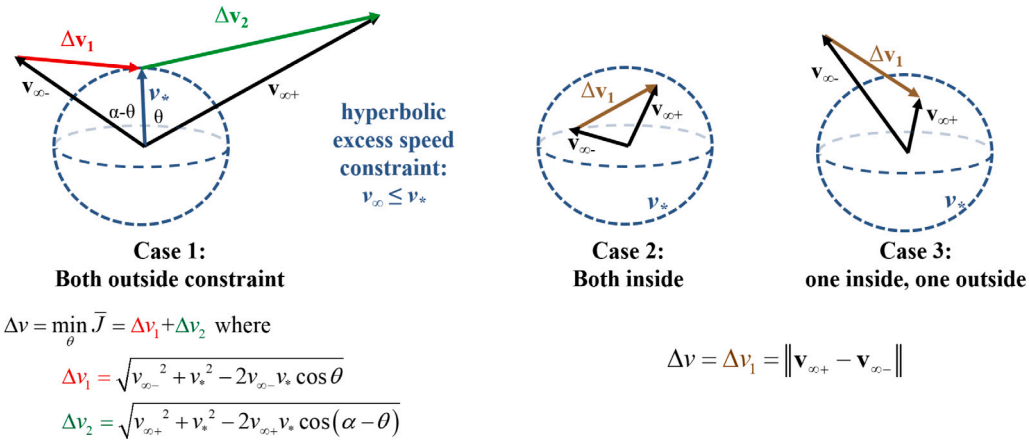

Fig. 6. Flyby maneuvers subject to maximum hyperbolic excess speed constraint.

The total statistics for the completed mothership itinerary are recorded, and a new search for another mothership can be initiated.

2.2.4. Broad search for mothership trajectories

Per the descriptions of the prior subsections, the Earth-to-asteroid selection requires two integer decision variables: the launch time step and which rank to choose for the first target. Each successive leg requires one integer decision variable: which rank to choose for the next target. In the final competition implementation, the launch time step is cycled in successive searches so that each step is equally considered. The rank selections for targets are chosen via a normally-distributed random number generator that assigns the higher ranked options with higher probabilities of selection. With more competition time, the team would have used a genetic algorithm or other global optimization method to make this choice.

Because the main compute effort of each search includes only Lambert solutions and precomputed lookup tables, 10 complete mothership trajectories can be computed in approximately one second of runtime on a single processor. As mothership scores improved, filters were put in place to terminate itineraries that had no chance of being a top performer, further increasing the efficiency of each search. The mothership searches are computed in parallel using multiple cores and multiple desktop servers, each using different seeds for the randomized rank selection. If the team had additional competition time, these searches would have been transitioned to a high-performance computing cluster. Ultimately, during the competition, the mothership searches were performed on approximately 30 cores for several days. Tens of thousands of high performing, feasible mothership trajectories were archived. Because each mothership was composed of optimized internal legs, the performance of each completed solution was immediately competitive with the posted scores from the leaderboard, reaching the order of magnitude of theoretical performance index ceiling from Fig. 1. However, improvement on mothership scores (i.e. convergence of the global solution) was quite slow due to the randomized rank choice approach. Improved performance of the overall solution would be expected with the use of a more informed global optimization algorithm.

2.2.5. Mass ratio estimator

An ATD propels the asteroid using the body's own mass; the mass flow for an asteroid i is constant in time and equal to $\dot{m}^i = \alpha\, m_0^i$, where m_0^i is the initial mass of asteroid i, and with $\alpha = 6 \times 10^{-9}$ s^{-1}. The mass delivered to the build-station is then $m_f^i = \max\left[0,\, m_0^i\,(1 - \alpha \Delta t)\right]$, where Δt is the transfer duration and m_0^i is the initial mass of asteroid i. The mass ratio m_r^i for asteroid i is defined as

$$m_r^i = \frac{m_f^i}{m_0^i}. \tag{4}$$

The mass ratio determines what fraction of the initial mass of an asteroid is delivered to the ring, effectively contributing to the final score.

The mass ratio depends on the asteroid's initial and final orbits, as well as on the phasing at the initial and final times, which are decided by the scheduler. Therefore, the mass ratios cannot be precisely known until a final solution is generated, but the generation of a trajectory shall use the mass ratio to be competitive. Hence, a way to quickly estimate the mass ratio is required.

The estimator is used to compute the cost-to-go in the mothership trajectory search as described in Section 2.2.3 and to select the 10 best mothership trajectories for a solution as discussed in Section 2.2.6. The estimator is trained using a subset of approximately three thousand combinations of asteroids and final ring orbits. The considered ring orbits have inclinations of zero radians, and semi-major axis varying between 0.9 and 1.3 AU, with a resolution of 0.1 AU. For each asteroid-ring pair, 144 minimum-time asteroid-to-ring trajectories are computed as in Section 2.3; every trajectory corresponds to a combination of 12 ring station phases and 12 build times. Since the scheduler described in Section 2.4 is efficient in maximizing the final mass of the asteroid, the best among the 144 trajectories is picked for every asteroid-ring combination. The estimator consists of a double linear interpolation: first, a linear regression between m_r and a_i is performed for every value of the asteroid ring semi-major axis a_{Dyson}; second, the slope and intercept are regressed as a function of a_{Dyson}. All other orbital parameters are neglected. The final model provides an estimated $\hat{m}_{r,i}(a_{\text{Dyson}})$ as a function of the ring orbit's semi-major axis.

2.2.6. Mothership trajectories selection

The approximate score is computed with a modified version of Eq. (2):

$$\hat{J} = B \frac{10^{-11} \frac{\sum_{i=1}^{n_k} \hat{m}_f^i}{12}}{a_{\text{Dyson}}^2 \left(1 + \frac{\Delta v_a N_a}{50}\right)^2} \tag{5}$$

where n_k is the number of asteroids reached by trajectory k, the estimated final mass of asteroid i is $\hat{m}_f^i = m_0^i\, \hat{m}_r^i(a_{\text{Dyson}})$, and $\hat{m}_r^i(a_{\text{Dyson}})$ is estimated according to Section 2.2.5. The computed mass for the expected score is an optimistic mass delivered on average to each station. The minimum mass per station cannot be used because it is not known.

Tens of thousands of mothership trajectories are generated according to Section 2.2.4. Only the best set of 10 trajectories are sought, per the problem constraints. A greedy search procedure selects 10 trajectories in 10 iterations and ensures no duplicate asteroids in different trajectories. Each iteration consists of the following steps:

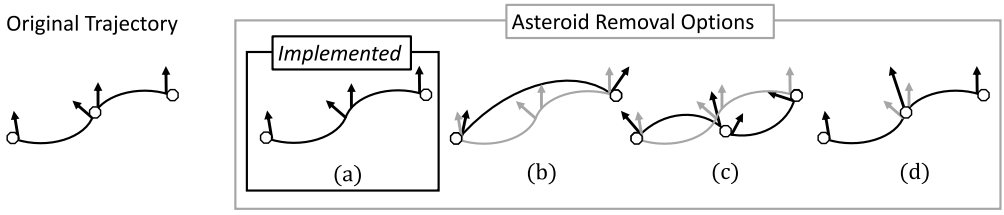

Fig. 7. Alternative asteroid removal strategies.

1. Compute an approximate score for each trajectory per Eq. (5).
2. Select the highest scoring trajectory, and label all the asteroids encountered by the selected trajectory.
3. Remove all the labeled asteroids from the trajectories that have not yet been selected, while leaving the corresponding impulsive maneuvers at the encounters.

The implemented strategy for removing asteroid orbits in step 3 is denoted option (a) in Fig. 7. For a given trajectory, option (a) only removes one asteroid while keeping the impulsive maneuvers at the encounter. If two consecutive asteroids were removed, the resulting trajectory could potentially have six impulsive maneuvers between asteroids, exceeding the allowable four impulsive maneuvers between asteroids.

After the competition ended, the search tool for minimizing impulsive maneuvers between flybys was developed further. The tool computes three more operations and the highest performing one is selected between (a)–(d) options including (b) remove the impulsive maneuver at the eliminated asteroid and link the neighboring asteroids with a solution to a Lambert problem; (c) substitute the eliminated flyby with a flyby of a nearby asteroid; and (d) simply compute a vector sum of the two maneuvers that occur at the missed encounter. For (c), multiple asteroids at multiple epochs are considered, and for (d), the Δv cost is the same if the maneuvers are collinear, otherwise the cost is always lowered. Fig. 7 shows the four asteroid removal methods.

2.2.7. Adding intermediate impulsive maneuvers

Some improvements to the mothership trajectories of the final solution were considered, but ultimately not used due to either time constraints or marginal benefit. One notable improvement incorporated intermediate impulsive maneuvers between asteroid flybys, defined here as a leg. The approach is similar to the technique presented in Refs. [9] and [10]. The final solution uses only one coast between two flybys. To consider the effect of more impulsive maneuvers, each leg of the submitted solution is discretized into 20 segments. The final positions and velocities of this leg and the total flight time are fixed. The 20 segments of the leg are designed to be position continuous relative to each other, but velocity discontinuous, necessitating the use of a solution to the two-body Lambert problem. For each leg, the magnitudes of these impulsive maneuvers are minimized in an unconstrained optimization algorithm, iterating on the 18 intermediate positions and using the same fixed flight time for every segment. The flight time of a segment is simply the overall flight time of the leg divided by 20.

Overall, the local optimization of each leg for the final solution showed marginal improvement. The new solution decreases the impulsive maneuver total from 146.1760 to 145.9726 km/s—a savings of only 0.2034 km/s or 0.1391%. Only 14 legs among hundreds of the final solution were improved. For these improved legs, the original structure was always Δv-Coast-Δv. The improved structure after optimization is one of three solutions: Coast-Δv-Coast-Δv, Δv-Coast-Δv-Coast, or Δv-Coast-Δv-Coast-Δv. See Fig. 8 for a visual on the structure of a general leg and the improvement steps. The result of this analysis confirms the efficiency of using ballistic arcs between targets for multi-body flyby or rendezvous missions when legs are on the order of half a revolution.

2.2.8. Incremental search

After the competition ended, a tool for incremental improvement of the mothership trajectories was developed. The key concept behind the tool is to exploit the highest performing trajectories and use them as initial guesses for an incremental search. As the problem is discontinuous, non-gradient based methods are necessary. Loosely inspired by simulated annealing [11], each iteration of the tool works as follows:

(1) Randomly select a leg of the trajectory.
(2) Compute the position of the mothership at 00:00 of every day, throughout the duration of the leg.
(3) For every computed position, search all asteroids within a pre-specified radius from the current mothership position.
(4) For every existing combination of neighboring asteroid and date, compute the following four modified trajectories where:
    (i) the asteroid is added
    (ii) the asteroid is added, and the previous encounter is removed
    (iii) the asteroid is added, and the following encounter is removed
    (iv) the asteroid is added, and both the preceding and following encounters are removed
(5) Compute, in addition, two more trajectories, with no added asteroids: one where the asteroid at the beginning of the leg is removed, and one where the asteroid at the end of the leg is removed.
(6) For every computed trajectory, the approximate score is computed.
(7) The trajectory for the next iteration is randomly selected from a pool consisting of all the newly computed trajectories and the original trajectory from the start of the iteration. Higher scoring trajectories are favored.

For step 3, precomputed 3-dimensional trees, one at 00:00 of every day, are employed to speed up the search. At step 4, the Lambert solver from [5,6] is used to compute the trajectories between the asteroids; the flybys are patched according to Fig. 6. If, after the modifications, a trajectory contains duplicates, the trajectory is deleted. For step 5, Eq. (5) is used. Finally, for step 6, the trajectories are selected according to:

$$p_k \propto e^{\hat{J}_k/T}, \tag{6}$$

where p_k is the probability for trajectory k to be picked, $\hat{J}_k$ is computed as in Eq. (5), and T is the temperature, a parameter that decreases at every major iteration according to:

$$T(j) = T_0 \left(1 - \frac{j}{N_{iter}}\right), \tag{7}$$

where j is the current major iteration number and N_{iter} is the total number of iterations; T_0 is a tuning parameter for the initial temperature.

The tool has been tested over a few mothership trajectories. To evaluate the performance, instead of solving the full problem, the contribution of each asteroid to the total score has been estimated via Eq. (5). In all cases, the trajectories were improved by around 300 points according to the linear estimator. Notably, this was true even

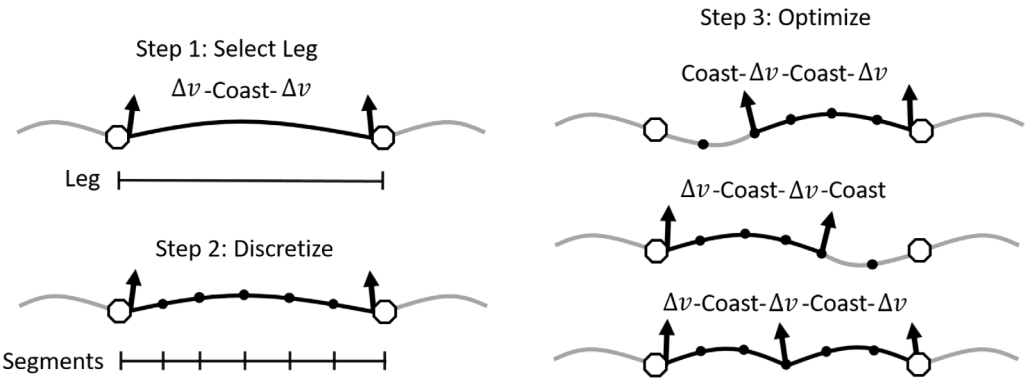

Fig. 8. The sequential steps of improving a trajectory leg of the mothership between asteroids. The arrows are impulsive maneuvers (Δv). The octagons are asteroids. The three portions of a trajectory on the right are the three optimal solutions encountered.

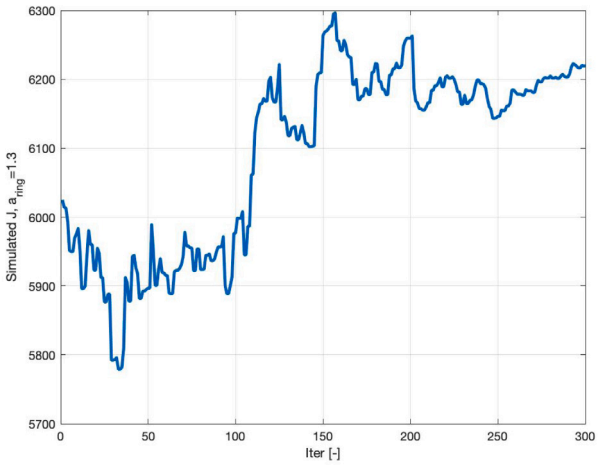

Fig. 9. Evolution of the estimated score for a single mothership trajectory using the incremental search tool, which was developed after the competition ended. The highest scoring trajectory has been used as initial guess. At every iteration, the score of the mothership trajectory is estimated with Eq. (5). $T_0 = 50$.

for the highest scoring trajectories. All newly generated trajectories had between one and three asteroid encounters more than the initial guess. It is worth noting that the timing of every single encounter had been changed by the tool, improving the solution. This is because, in the original mothership trajectory search, the encounter time is optimized keeping into account the trajectory up to the encounter and neglecting the following steps. Fig. 9 shows the evolution of the estimated score using the described tool for 300 major iterations, in the case where the team's single highest scoring mothership trajectory is used as the initial guess. The initial guess has a value higher than the final score of the team because it is the score of the single highest scoring mothership trajectory.

2.3. Asteroid-to-ring trajectory search

The output of the mothership trajectory search includes a list of asteroids to send to build-stations on the Dyson ring. The goal of the asteroid-to-ring trajectory search and scheduler is to compute constant-thrust-acceleration transfers for all selected asteroids to the build-stations, choose which asteroids to send to which build-stations, and to choose the build-station construction order. Each asteroid can arrive at any of the 12 build-stations at any of the 12 instantaneous arrival times. The 12 arrival times are defined as follows: Working backwards from the final arrival time of 103044 MJD, the remaining eleven arrival times are spaced sequentially 91 days apart such that the earliest arrival time is 102043 MJD.

2.3.1. Indirect method necessary conditions

All the indirect optimization problems discussed here are constant-thrust-acceleration trajectories from one orbit to another. Only the last presented set of necessary conditions is actually used to generate solutions, but the other sets of necessary conditions are included because they may be useful in other contexts and provide insight into indirect optimization for constant-thrust-acceleration spacecraft trajectories.

Each asteroid-to-ring trajectory is a transfer from a natural asteroid orbit to a build-station orbit. The dynamics along the asteroid-to-ring trajectory are governed by the point-mass gravitational attraction of the Sun and an additional constant-magnitude thrust acceleration provided by the ATD. The equations of motion,

$$\mathbf{f}(\mathbf{x},\mathbf{u}) = \begin{bmatrix}\dot{\mathbf{r}}\\ \dot{\mathbf{v}}\end{bmatrix} = \begin{bmatrix}\mathbf{v}\\ -\mu\frac{\mathbf{r}}{\|\mathbf{r}\|^3} + \Gamma_{\mathrm{ATD}}\hat{\mathbf{q}}\end{bmatrix} \tag{8}$$

are formulated with position $\mathbf{r}$ and velocity $\mathbf{v}$ in the J2000 inertial heliocentric ecliptic coordinate frame. The gravitational potential of the Sun is $\mu = 1.32712440018 \times 10^{11}$ km^3/s^2. The unit vector $\hat{\mathbf{q}}$ defines the direction of the thrust and $\Gamma_{\mathrm{ATD}} = 1 \times 10^{-4}$ m/s^2 is the magnitude of the thrust acceleration. The states of the system are $\mathbf{x} = \left[\mathbf{r}^T, \mathbf{v}^T\right]^T$ and the controls of the system are $\mathbf{u} = \hat{\mathbf{q}}$.

The initial time for the trajectory is t_0 and the final time is t_f. The general expressions for the initial and final constraints are denoted $\boldsymbol{\theta}(\mathbf{x}_0, t_0) = 0$ and $\boldsymbol{\psi}(\mathbf{x}_f, t_f) = 0$, respectively. The notation $\mathbf{x}_0 = \mathbf{x}(t_0)$ and $\mathbf{x}_f = \mathbf{x}(t_f)$ is used where appropriate for conciseness.

Since the asteroid is transferred to the build-station with a constant-thrust acceleration and a constant mass consumption rate, the minimum-time-of-flight solution maximizes the asteroid mass at the

build-station arrival. The performance index for the minimum-time-of-flight solution is

$$J_t = t_f - t_0. \tag{9}$$

The equations of motion and the constraints are incorporated into the performance index to form the augmented performance index

$$J_t' = J_t + \boldsymbol{\eta}^T \boldsymbol{\theta}(\mathbf{x}_0, t_0) + \boldsymbol{\nu}^T \boldsymbol{\psi}(\mathbf{x}_f, t_f) + \int_{t_0}^{t_f} \left[\boldsymbol{\lambda}^T \left(\mathbf{f}(\mathbf{x}, \mathbf{u}) - \dot{\mathbf{x}}\right)\right] dt. \tag{10}$$

The quantities $\boldsymbol{\eta}$, $\boldsymbol{\nu}$, and $\boldsymbol{\lambda}$ are Lagrange multipliers introduced for the initial constraints, final constraints, and equations of motion, respectively. The Lagrange multipliers for the equations of motion are also referred to as the co-states. The augmented performance index is expressed in terms of the functions $G(\mathbf{x}_0, \mathbf{x}_f, t_0, t_f)$ and $H(\mathbf{x}, \mathbf{u}, \boldsymbol{\lambda})$:

$$J_t' = G(\mathbf{x}_0, \mathbf{x}_f, t_0, t_f) + \int_{t_0}^{t_f} \left[H(\mathbf{x}, \mathbf{u}, \boldsymbol{\lambda}) + \boldsymbol{\lambda}^T \dot{\mathbf{x}}\right] dt, \tag{11}$$

where

$$G(\mathbf{x}_0, \mathbf{x}_f, t_0, t_f) = J_t + \boldsymbol{\eta}^T \boldsymbol{\theta}(\mathbf{x}_0, t_0) + \boldsymbol{\nu}^T \boldsymbol{\psi}(\mathbf{x}_f, t_f), \tag{12}$$

$$H(\mathbf{x}, \mathbf{u}, \boldsymbol{\lambda}) = \boldsymbol{\lambda}^T \mathbf{f}(\mathbf{x}, \mathbf{u}). \tag{13}$$

The function $H(\mathbf{x}, \mathbf{u}, \boldsymbol{\lambda})$ is also known as the Hamiltonian. Setting the differential dJ_t' to zero yields the Euler–Lagrange equations, which provide the following set of boundary (or transversality) conditions,

$$\boldsymbol{\lambda}_0^T = -\frac{\partial G}{\partial \mathbf{x}_0}, \quad H_0 = \frac{\partial G}{\partial t_0}, \quad \boldsymbol{\lambda}_f^T = \frac{\partial G}{\partial \mathbf{x}_f}, \quad H_f = -\frac{\partial G}{\partial t_f}, \tag{14}$$

on the co-states and the Hamiltonian. The Euler–Lagrange equations also provide the equations of motion for the co-states,

$$\dot{\boldsymbol{\lambda}} = -\frac{\partial H}{\partial \mathbf{x}}. \tag{15}$$

The Lagrange multipliers $\boldsymbol{\lambda} = \left[\boldsymbol{\lambda}_{\mathbf{r}}^T, \boldsymbol{\lambda}_{\mathbf{v}}^T\right]^T$ are composed of three co-states for position $\boldsymbol{\lambda}_{\mathbf{r}}$, and three co-states for velocity, $\boldsymbol{\lambda}_{\mathbf{v}}$. Expressing the Hamiltonian explicitly in terms of the position and velocity co-states, and substituting $\mathbf{f}(\mathbf{x}, \mathbf{u})$ from Eq. (8) yields

$$H(\mathbf{x}, \mathbf{u}, \boldsymbol{\lambda}_{\mathbf{r}}, \boldsymbol{\lambda}_{\mathbf{v}}) = \boldsymbol{\lambda}_{\mathbf{r}}^T \mathbf{v} + \boldsymbol{\lambda}_{\mathbf{v}}^T \left(-\mu \frac{\mathbf{r}}{\|\mathbf{r}\|^3} + \Gamma_{\text{ATD}} \hat{\mathbf{q}}\right). \tag{16}$$

According to Pontryagin's minimum/maximum principle [12] as well as the Weierstrass condition [13], the optimal control $\mathbf{u} = \hat{\mathbf{q}}$ must necessarily minimize the Hamiltonian. Therefore, by inspection of Eq. (16), the optimal control is

$$\hat{\mathbf{q}} = -\frac{\boldsymbol{\lambda}_{\mathbf{v}}}{\|\boldsymbol{\lambda}_{\mathbf{v}}\|}. \tag{17}$$

Substituting Eq. (17) into Eq. (16) and simplifying,

$$H(\mathbf{x}, \mathbf{u}, \boldsymbol{\lambda}_{\mathbf{r}}, \boldsymbol{\lambda}_{\mathbf{v}}) = \boldsymbol{\lambda}_{\mathbf{r}}^T \mathbf{v} - \boldsymbol{\lambda}_{\mathbf{v}}^T \mathbf{r} \frac{\mu}{\|\mathbf{r}\|^3} - \|\boldsymbol{\lambda}_{\mathbf{v}}\| \Gamma_{\text{ATD}}. \tag{18}$$

The initial and final boundary conditions are

$$\boldsymbol{\theta}(\mathbf{r}_0, \mathbf{v}_0, t_0) = \begin{bmatrix} \mathbf{r}_0 - \mathbf{r}_D(t_0) \\ \mathbf{v}_0 - \mathbf{v}_D(t_0) \end{bmatrix}, \quad \boldsymbol{\psi}(\mathbf{r}_f, \mathbf{v}_f, t_f) = \begin{bmatrix} \mathbf{r}_f - \mathbf{r}_A(t_f) \\ \mathbf{v}_f - \mathbf{v}_A(t_f) \end{bmatrix}. \tag{19}$$

where $\mathbf{r}_D(t_0)$ and $\mathbf{v}_D(t_0)$ are the position and velocity of the natural asteroid departure orbit at the initial time and $\mathbf{r}_A(t_f)$ and $\mathbf{v}_A(t_f)$ are the position and velocity of the build-station arrival orbit at the final time. The departure and arrival orbits follow Keplerian two-body dynamics.

The function $G(\mathbf{x}_0, \mathbf{x}_f, t_0, t_f)$ can be expressed as

$$\begin{aligned} G(\mathbf{r}_0, \mathbf{v}_0, \mathbf{r}_f, \mathbf{v}_f, t_0, t_f) = J_t &+ \boldsymbol{\eta}_{\mathbf{r}}^T \left[\mathbf{r}_0 - \mathbf{r}_D(t_0)\right] + \boldsymbol{\eta}_{\mathbf{v}}^T \left[\mathbf{v}_0 - \mathbf{v}_D(t_0)\right] \\ &+ \boldsymbol{\nu}_{\mathbf{r}}^T \left[\mathbf{r}_f - \mathbf{r}_A(t_f)\right] + \boldsymbol{\nu}_{\mathbf{v}}^T \left[\mathbf{v}_f - \mathbf{v}_A(t_f)\right], \end{aligned} \tag{20}$$

where the Lagrange multipliers $\boldsymbol{\eta} = \left[\boldsymbol{\eta}_{\mathbf{r}}^T, \boldsymbol{\eta}_{\mathbf{v}}^T\right]^T$ for the initial state are composed of three position components $\boldsymbol{\eta}_{\mathbf{r}}$, and three velocity components $\boldsymbol{\eta}_{\mathbf{v}}$. The final constraint Lagrange multipliers $\boldsymbol{\nu} = \left[\boldsymbol{\nu}_{\mathbf{r}}^T, \boldsymbol{\nu}_{\mathbf{v}}^T\right]^T$ are similarly composed of position and velocity components.

The transversality conditions from Eq. (14) become

$$\boldsymbol{\lambda}_{\mathbf{r}_0}^T = -\boldsymbol{\eta}_r^T, \quad \boldsymbol{\lambda}_{\mathbf{v}_0}^T = -\boldsymbol{\eta}_v^T. \tag{21}$$

The second transversality condition from Eq. (14) becomes

$$H_0 = -1 - \boldsymbol{\eta}_r^T \frac{\partial \mathbf{r}_D(t_0)}{\partial t_0} - \boldsymbol{\eta}_v^T \frac{\partial \mathbf{v}_D(t_0)}{\partial t_0}. \tag{22}$$

When the initial constraint is satisfied, the derivatives of the departure orbit position and velocity match the equations of motion (excluding the additional constant acceleration term). Therefore

$$H_0 = -1 - \boldsymbol{\eta}_r^T \mathbf{v}_0 + \boldsymbol{\eta}_v^T \mathbf{r}_0 \frac{\mu}{\|\mathbf{r}_0\|^3}, \tag{23}$$

and, after substituting Eq. (21) into Eq. (23),

$$H_0 = -1 + \boldsymbol{\lambda}_{\mathbf{r}_0}^T \mathbf{v}_0 - \boldsymbol{\lambda}_{\mathbf{v}_0}^T \mathbf{r}_0 \frac{\mu}{\|\mathbf{r}_0\|^3}. \tag{24}$$

Comparing Eq. (24) to the expression for the Hamiltonian from Eq. (18) evaluated at the initial time,

$$H_0 = -\|\boldsymbol{\lambda}_{\mathbf{v}_0}\| \Gamma_{\text{ATD}} + \boldsymbol{\lambda}_{\mathbf{r}_0}^T \mathbf{v}_0 - \boldsymbol{\lambda}_{\mathbf{v}_0}^T \mathbf{r}_0 \frac{\mu}{\|\mathbf{r}_0\|^3}, \tag{25}$$

the magnitude of the initial velocity co-state must be

$$\|\boldsymbol{\lambda}_{\mathbf{v}_0}\| = \frac{1}{\Gamma_{\text{ATD}}}. \tag{26}$$

Also, starting with the transversality conditions in Eqs. (14), the magnitude of the final velocity co-state is constrained to the same value

$$\|\boldsymbol{\lambda}_{\mathbf{v}_f}\| = \frac{1}{\Gamma_{\text{ATD}}}. \tag{27}$$

Using a forward-shooting method, the decision-state vector and constraint vector for the TPBVP are

$$\mathbf{U}_{8\times1}^{(A)} = \begin{bmatrix} \boldsymbol{\lambda}_{\mathbf{r}_0}^T & \boldsymbol{\lambda}_{\mathbf{v}_0}^T & t_0 & t_f \end{bmatrix}^T, \quad \mathbf{C}_{8\times1}^{(A)} = \begin{bmatrix} \mathbf{r}_f - \mathbf{r}_A(t_f) \\ \mathbf{v}_f - \mathbf{v}_A(t_f) \\ \|\boldsymbol{\lambda}_{\mathbf{v}_0}\| - \frac{1}{\Gamma_{\text{ATD}}} \\ \|\boldsymbol{\lambda}_{\mathbf{v}_f}\| - \frac{1}{\Gamma_{\text{ATD}}} \end{bmatrix}. \tag{28}$$

The equations of motion for the co-states are found by taking the partial derivatives specified in Eq. (15),

$$\dot{\boldsymbol{\lambda}}_{\mathbf{r}} = \frac{\mu}{\|\mathbf{r}\|^5} \left[\|\mathbf{r}\|^2 \boldsymbol{\lambda}_{\mathbf{v}} - 3(\boldsymbol{\lambda}_{\mathbf{v}}^T \mathbf{r})\mathbf{r}\right], \tag{29}$$

$$\dot{\boldsymbol{\lambda}}_{\mathbf{v}} = -\boldsymbol{\lambda}_{\mathbf{r}}. \tag{30}$$

The TPBVP as defined in Eq. (28) has eight unknowns and eight constraints. The dimensionality of the TPBVP can reduced by expressing the direction of the initial velocity co-state as a pair of spherical coordinates λ_{α_0}, λ_{β_0} such that,

$$\hat{\boldsymbol{\lambda}}_{\mathbf{v}_0} = \begin{bmatrix} \cos\lambda_{\alpha_0} \cos\lambda_{\beta_0} & \cos\lambda_{\alpha_0} \sin\lambda_{\beta_0} & \sin\lambda_{\alpha_0} \end{bmatrix}^T, \tag{31}$$

with $\boldsymbol{\lambda}_{\mathbf{v}_0} = \hat{\boldsymbol{\lambda}}_{\mathbf{v}_0} / \Gamma_{\text{ATD}}$, ensuring that the magnitude of the initial velocity co-state vector meets the transversality condition from Eq. (26). Automatically enforcing the constraint on the initial velocity co-state magnitude reduces the size of the problem to seven unknowns and constraints.

$$\mathbf{U}_{7\times1}^{(B)} = \begin{bmatrix} \boldsymbol{\lambda}_{\mathbf{r}_0}^T & \lambda_{\alpha_0} & \lambda_{\beta_0} & t_0 & t_f \end{bmatrix}^T, \quad \mathbf{C}_{7\times1}^{(B)} = \begin{bmatrix} \mathbf{r}_f - \mathbf{r}_A(t_f) \\ \mathbf{v}_f - \mathbf{v}_A(t_f) \\ \|\boldsymbol{\lambda}_{\mathbf{v}_f}\| - \frac{1}{\Gamma_{\text{ATD}}} \end{bmatrix}. \tag{32}$$

Because the acceleration is constant in the direction of $\boldsymbol{\lambda}_{\mathbf{v}}$, motion of the spacecraft is completely invariant to the magnitude of $\boldsymbol{\lambda}$. The minimum-time-of-flight transversality conditions only require that the magnitudes of the initial and final velocity co-states match. Therefore, the co-states can be scaled by constant k, which is equivalent to solving

the scaled minimum-time-of-flight problem $J_t' = k(t_f - t_0)$. Setting $k = \Gamma_{\text{ATD}}$, the TPBVP can be equivalently implemented as

$$\mathbf{U}_{7\times1}^{(C)} = \begin{bmatrix} \lambda_{\mathbf{r}_0}^T & \lambda_{\alpha_0} & \lambda_{\beta_0} & t_0 & t_f \end{bmatrix}^T, \quad \mathbf{C}_{7\times1}^{(C)} = \begin{bmatrix} \mathbf{r}_f - \mathbf{r}_A(t_f) \\ \mathbf{v}_f - \mathbf{v}_A(t_f) \\ \|\lambda_{\mathbf{v}_f}\| - 1 \end{bmatrix}. \tag{33}$$

with $\lambda_{\mathbf{v}_0} = \hat{\lambda}_{\mathbf{v}_0}$ automatically enforced, and the scaling of the TPBVP is improved because all of the constraints are of order unity.

If the final time is fixed and the initial time remains free, the TPBVP from Eq. (33) becomes,

$$\mathbf{U}_{6\times1}^{(D)} = \begin{bmatrix} \lambda_{\mathbf{r}_0}^T & \lambda_{\alpha_0} & \lambda_{\beta_0} & t_0 \end{bmatrix}^T, \quad \mathbf{C}_{6\times1}^{(D)} = \begin{bmatrix} \mathbf{r}_f - \mathbf{r}_A(t_f) \\ \mathbf{v}_f - \mathbf{v}_A(t_f) \end{bmatrix}. \tag{34}$$

with $\lambda_{\mathbf{v}_0} = \hat{\lambda}_{\mathbf{v}_0}$ automatically enforced. When the final time is fixed, the boundary condition for the magnitude of $\lambda_{\mathbf{v}_f}$ no longer exists.

The minimum-time-of-flight solutions with free initial time and free final time preserve the most possible mass upon arrival at the build-station. However, in the chosen solution methodology, the asteroids are only allowed to arrive at the build-stations during the 12 fixed build-station arrival times. Therefore, the actual TPBVP implemented for the GTOC11 solution uses a free initial time at the departure (asteroid) orbit, and a fixed final time at the arrival (build-station) orbit. In preliminary experiments, more reliable convergence was achieved when performing backwards-shooting, so the TPBVP was implemented using backwards-shooting rather than forward-shooting. The decision-state vector and constraint vector actually employed for the GTOC11 asteroid-to-ring trajectory search are:

$$\mathbf{U}_{7\times1}^{(E)} = \begin{bmatrix} \lambda_{\mathbf{r}_f}^T & \lambda_{\mathbf{v}_f}^T & t_0 \end{bmatrix}^T, \quad \mathbf{C}_{6\times1}^{(E)} = \begin{bmatrix} \mathbf{r}_0 - \mathbf{r}_D(t_0) \\ \mathbf{v}_0 - \mathbf{v}_D(t_0) \end{bmatrix}. \tag{35}$$

The decision-state vector $\mathbf{U}_{7\times1}^{(E)}$ has seven elements, but due to the invariance to the scaling of λ noted above, the decision-state space is only six-dimensional, making the TPBVP square.

2.3.2. Two-point boundary value problem solver

The asteroid-to-ring trajectory search tool was developed in Fortran during the GTOC11 competition using message passing interface (MPI) parallelization on the high-performance Stampede2 compute nodes at the Texas Advanced Computing Center (TACC). Asteroid-to-ring trajectories are computed for every possible combination of asteroid, build-station, and arrival time using the indirect solver.

The initial guesses for the co-states $\lambda_{\mathbf{r}_f}$, $\lambda_{\mathbf{v}_f}$ and initial time t_0 are chosen by selecting the sample with the highest performance index from 1000 random samples of the decision-state vector. The guesses for the final co-states are drawn from the uniform distribution $U(-5, 5)$. The guesses for the initial times t_0 are determined by subtracting a random fraction of the asteroid orbit period from the fixed final time, where the random fraction is drawn from the uniform distribution $U(0, \rho)$. The quantity ρ is a multiplier for the asteroid orbit period that starts at $\rho = 0.75$. The multiplier ρ is increased by a factor of 1.25 when a solution fails to converge in order to bias the decision-state initial guess towards longer times-of-flight on subsequent attempts.

The trajectories are calculated by back-propagating the equations of motion specified in Eq. (8) and Eqs. (29)–(30) from the arrival time t_f to the departure time t_0. The integrator uses an adaptive step-size with 7(8)th order Runge–Kutta-Fehlberg coefficients [14]. The two-point boundary problem is solved using a second-order Levenberg–Marquardt step-length-based trust region method [15,16]. The first-order Jacobian is found using complex-step differentiation and the second-order Hessian is found using a three-point central finite difference of the first-order complex-step derivatives.

The asteroid-to-ring trajectory solver is configured to run on 51 Knights Landing (KNL) compute nodes using 3420 MPI tasks for two hours.[3] For the submitted solution, 38448 total asteroid-to-ring trajectories are attempted. A total of 98.6% of the attempted solutions successfully converge after a maximum of ten attempts.

2.4. Build-station arrival scheduler

Each transfer output by the asteroid-to-ring trajectory solver connects the asteroid's natural orbit to one of the 12 build-stations, with the arrival occurring during one of the 12 available arrival times. The goals of the build-station scheduler are to select the build-station order and the allocation of asteroids to build-stations that yields the highest GTOC11 performance index from Eq. (1).

The mass of each asteroid upon arrival at the build-stations is determined from the mass depletion rate and the transfer time-of-flight. The asteroid transfers are filtered for initial times t_0 that occur before each asteroid's mothership encounter and for times-of-flight that are long enough to deplete the entire asteroid mass.

Given a candidate build-station arrival order and a set of valid asteroid transfers from the asteroid-to-ring trajectory solver, an iterative process is taken to match asteroids to build-stations. First, only solutions that arrive at the build-stations according to the build-station arrival order are considered. Then the build-station with the least accumulated mass is considered and an asteroid transfer to that station is selected, removing all other transfers of that asteroid. The process is repeated, assigning asteroid transfers to the build-station with the least accumulated mass at each step, as illustrated in Fig. 10. Once there are no remaining asteroid transfers to assign, the GTOC11 performance index from Eq. (1) is computed.

The asteroid-to-ring transfer assignment process explained above is repeated for many candidate build-station arrival orders, seeking the build-station arrival order that yields the best performance index value. A modified version of the Non-Dominated Sorting Genetic Algorithm II (NSGA-II) is employed to select the build-station arrival order [17]. A population of N individuals formed by randomly permuting the numbers from 1–12 is used as the initial generation. These individuals are evaluated and then a bi-modal tournament selection is used to choose one quarter of the population as parents to make the child generation. The child generation is created by randomly permuting 1, 4, and 6 genes of the parent as well as flipping each parent at a random gene location. Standard crossover is not used, as it would not guarantee that each station is in the resulting genome. After being formed, the child generation is evaluated and combined with the parent generation for sorting. The best N individuals of the combined child + parent generation are chosen to be the parents of the next generation. This process is then repeated until the best solution has remained constant for 20 generations, at which point the algorithm is considered to be converged.

An early implementation of the build-station arrival scheduler used the best solution from a large sample of random permutations of the build-station arrival order, rather than using a genetic algorithm. By applying the genetic algorithm, the performance index improved by about 100 points, which was a substantial improvement in the critical final hours of the competition.

2.4.1. Future work

A number of improvements to the solution methodology could be made. The search space over the geometry of the build-station ring is not fully explored, specifically the build-station orbit-plane orientation. The mothership trajectory generation and selection methodology could be improved by incorporating global optimization methods for choosing the next target, as opposed to the current bias randomized choice method. The current mothership trajectory generation method stacks locally optimal single legs, but does not optimize complete end-to-end

[3] Specifications at: https://portal.tacc.utexas.edu/user-guides/stampede2

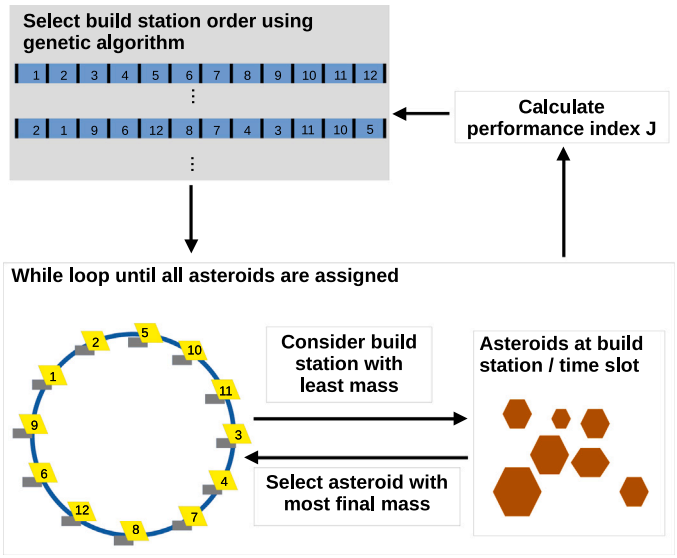

Fig. 10. Build-station scheduler schematic.

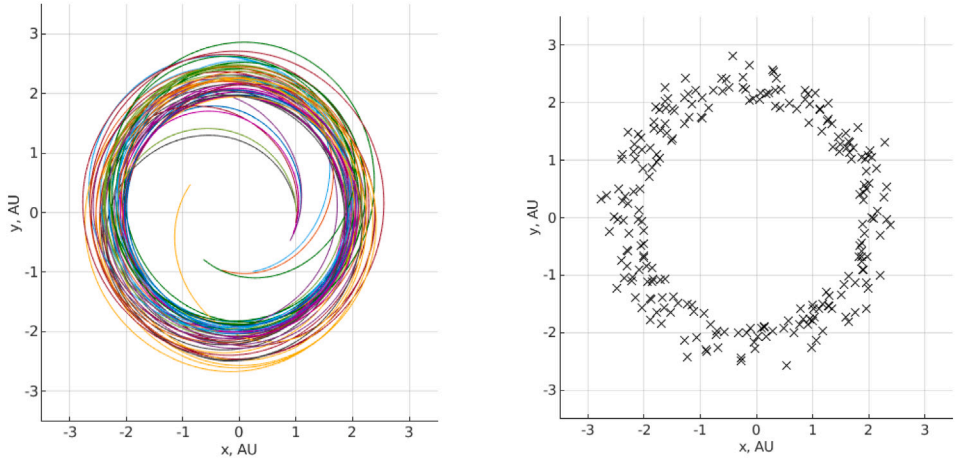

(a) Mothership trajectories (b) Mothership-asteroid encounters

Fig. 11. Mothership itineraries. (For interpretation of the references to color in this figure legend, the reader is referred to the web version of this article.)

multiple-leg trajectories, an obvious next step given more competition time. The mothership trajectory search could be further improved by taking advantage of available high-performance computing (HPC) resources to generate more candidate solutions quickly rather than relying on personal workstations.

The indirect solver used to generate asteroid-to-ring trajectories does take advantage of the HPC resources available to the UT Austin team, enabling a significant reduction in solution generation time with MPI parallelization. The indirect optimization method is formulated using Cartesian coordinates, but the efficiency of the solver could be improved by selecting more natural orbital element coordinates. The solution methodology relies on the asteroids reaching the build-stations during 12 instantaneous arrival times, fixing the final times for the indirect optimization problems, and resulting in solutions that are suboptimal compared to the free initial and final time, minimum-time-of-flight solutions. A better solution methodology would widen the build-station arrival time windows, allowing truly optimal transfers.

Table 1
Summary data for final submitted solution.

J	5885.469300
M_{min}	1.13283×10^{15} kg
N	235 asteroids
a_{Dyson}	1.1 AU
i_{Dyson}, Ω_{Dyson}, $\phi_{\text{Dyson,1}}$	0 radians

3. Results

Table 1 shows overview data for the final submitted solution. The symbol N represents the total number of asteroids encountered. The average Δv cost per flyby is 0.5556 km/s.

Figs. 11–12 show selected geometric characteristics of the final submitted solution using a top view in the J2000 inertial heliocentric frame. Fig. 11(a) shows the mothership trajectories. Each line representing a mothership trajectory is assigned a unique color. Fig. 11(b) shows the locations of all mothership-asteroid encounters.

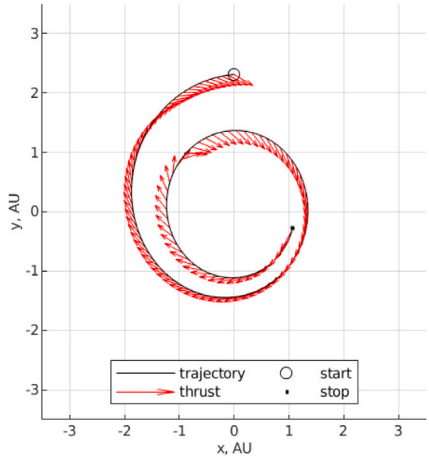

Fig. 12. Example constant-thrust-acceleration asteroid-to-ring transfer.

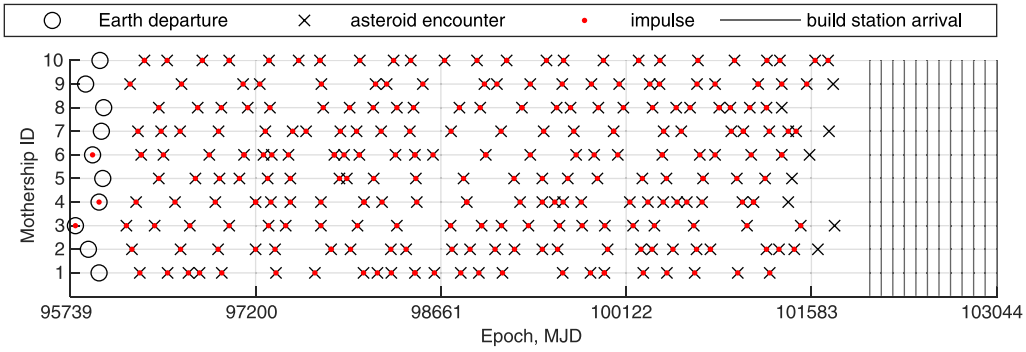

Fig. 13. Mothership trajectory timeline.

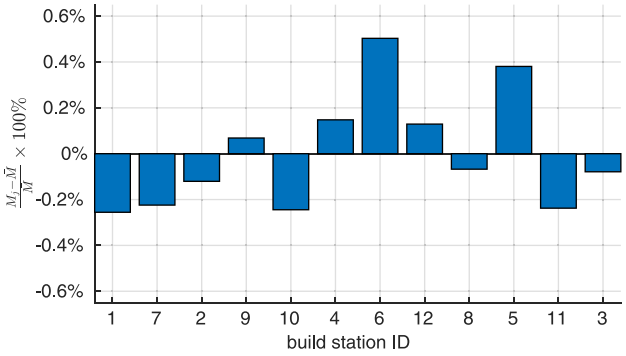

Fig. 14. Build-station mass distribution.

Fig. 12 shows the constant acceleration asteroid-to-ring transfer for an arbitrarily selected asteroid from the solution. Fig. 12 shows the transfer for asteroid 83336, which is encountered by mothership 10 and travels to build-station one.

Fig. 13 shows a timeline of the mothership itineraries, indicating the epochs when the motherships depart from Earth, when they encounter each asteroid, when the motherships perform impulsive maneuvers, and when the asteroids arrive at the build-stations. All impulses are performed immediately before and/or after encounters with asteroids or immediately following Earth departure. Impulses only occur at the final encounters when they are required to meet the 2 km/s relative speed requirement for rendezvous. The final encounters for each mothership occur about three years before the final epoch of 103044 MJD because asteroids that would be encountered after this point do not have enough time to transfer to the build-station.

Fig. 14 illustrates the variation of asteroid mass delivered to each build-station. Each bar represents the percent difference between the build-station mass and the mean mass among all build-stations. The order of build-station IDs listed in Fig. 14 corresponds to the order in which the build-stations are constructed.

This article includes a supplementary video file illustrating the final submitted solution from the UT Austin GTOC11 team. The supplementary video shows all mothership and asteroid trajectories during the 20 year mission, and it indicates the locations where the motherships perform maneuvers as well as where the mothership-asteroid encounters occur.

4. Conclusions

The UT Austin team placed fourth on the GTOC11 leaderboard with the solution presented above. The solution is developed by generating and selecting mothership-to-asteroid trajectories, solving for constant acceleration asteroid-to-ring trajectories, scheduling the build-station construction sequence, and assigning asteroids to build-stations to maximize the performance index.

The GTOC11 competition was an exciting and educational experience for the UT Austin team. During the design and execution of the solution methodology, a number of new techniques and insights were made that may be useful to the broader field of trajectory optimization, mission design, and space situational awareness. Notable such contributions include the bounding box discretization scheme combined with precomputed ephemerides, the model reduction strategy for sequencing, and the detailed treatment of the necessary conditions and associated subtleties of the indirect optimization problem.

Declaration of competing interest

The authors declare that they have no known competing financial interests or personal relationships that could have appeared to influence the work reported in this paper.

Acknowledgments

The authors recognize the contributions from the entire GTOC11 UT Austin student team, including David Cunningham, Courtney Hollenberg, Chun-Yi Wu, and Burton Yale. The authors thank the anonymous peer-reviewers for their insightful feedback. The authors acknowledge the Texas Advanced Computing Center (TACC) at The University of Texas at Austin for providing high-performance computing resources that have contributed to the results reported within this paper. http://www.tacc.utexas.edu. This research did not receive any specific grant from funding agencies in the public, commercial, or not-for-profit sectors. Finally, the authors wish to congratulate the host team, the winning team, and other participating teams.

Appendix A. Supplementary data

Supplementary material related to this article can be found online at https://doi.org/10.1016/j.actaastro.2022.07.007.

References

[1] H.-X. Shen, Y.-Z. Luo, Y.-H. Zhu, A.-Y. Huang, Dyson sphere building: On the design of the GTOC11 problem and summary of the results, Acta Astronaut. (2022) (in this issue).
[2] Global trajectory optimization competition (GTOC) portal, 2022, https://sophia.estec.esa.int/gtoc_portal/. (Accessed 24 June 2022).
[3] D. Izzo, 1st ACT global trajectory optimisation competition: Problem description and summary of the results, Acta Astronaut. 61 (9) (2007) 731–734, http://dx.doi.org/10.1016/j.actaastro.2007.03.003.
[4] X. Huang, B. Yang, P. Sun, S. Li, H. Yang, 10th China trajectory optimization competition: Problem description and summary of the results, Astrodynamics 5 (1) (2021) 1–11, http://dx.doi.org/10.1007/s42064-020-0089-2.
[5] R.P. Russell, On the solution to every Lambert problem, Celestial Mech. Dynam. Astronom. 131 (11) (2019) 1–33, http://dx.doi.org/10.1007/s10569-019-9927-z.
[6] R.P. Russell, Complete Lambert solver including second-order sensitivities, J. Guid. Control Dyn. 45 (2) (2022) 196–212, http://dx.doi.org/10.2514/1.G006089.
[7] E. Borgonovo, Sensitivity analysis, an introduction for the management scientist, in: International Series in Operations Research & Management Science, Springer, 2017, pp. 1–7, http://dx.doi.org/10.1007/978-3-319-52259-3.
[8] N. Arora, R.P. Russell, A fast, accurate, and smooth planetary ephemeris retrieval system, Celestial Mech. Dynam. Astronom. 108 (2) (2010) 107–124, http://dx.doi.org/10.1007/s10569-010-9296-0.
[9] L.A. D'Amario, D.V. Byrnes, R.H. Stanford, A new method for optimizing multiple-flyby trajectories, J. Guid. Control Dyn. 4 (5) (1981) 591–596, http://dx.doi.org/10.2514/3.56115.
[10] D. Ottesen, R.P. Russell, Unconstrained direct optimization of spacecraft trajectories using many embedded Lambert problems, J. Optim. Theory Appl. (2021) 1–41, http://dx.doi.org/10.1007/s10957-021-01884-1.
[11] S. Kirkpatrick, C.D. Gelatt Jr., M.P. Vecchi, Optimization by simulated annealing, Science 220 (4598) (1983) 671–680, http://dx.doi.org/10.1126/science.220.4598.671.
[12] L.S. Pontryagin, V.G. Boltyanskii, R.V. Gamkrelidze, E.F. Mishchenko, The mathematical theory of optimal processes, in: L.W. Neustadt (Ed.), L.S. Pontryagin Selected Works, Gordon and Breach Science Publishers, 1986, pp. 17–21.
[13] D.G. Hull, Optimal Control Theory for Applications, Springer Science & Business Media, 2013, p. 167.
[14] E. Fehlberg, Classical Fifth-, Sixth-, Seventh-, and Eighth-Order Runge-Kutta Formulas with Stepsize Control, Tech. Rep., (TR R-287) George C. Marshall Space Flight Center, 1968.
[15] K. Levenberg, A method for the solution of certain non-linear problems in least squares, Quart. Appl. Math. 2 (2) (1944) 164–168, http://dx.doi.org/10.1090/qam/10666.
[16] D.W. Marquardt, An algorithm for least-squares estimation of nonlinear parameters, J. Soc. Ind. Appl. Math. 11 (2) (1963) 431–441, http://dx.doi.org/10.1137/0111030.
[17] K. Deb, A. Pratap, S. Agarwal, T. Meyarivan, A fast and elitist multiobjective genetic algorithm: NSGA-II, IEEE Trans. Evol. Comput. 6 (2) (2002) 182–197, http://dx.doi.org/10.1109/4235.996017.